Pyrolysis products from industrial waste biomass based on a neural network model

Yifei Sun[a, c, *], Lina Liu[b, c], Qiang Wang[b, c], Xiaoyi Yang[b, c], Xin Tu[d]

[a] Beijing Key Laboratory of Bio-inspired Energy Materials and Devices, School of Space and Environment, Beihang University, 37 Xueyuan Road, Haidian District, Beijing, 100191, China

[b] School of Energy and Power Engineering, Beihang University, 37 Xueyuan Road, Haidian District, Beijing, 100191, China

[c] Energy and Environment International Centre, Beihang University, 37 Xueyuan Road, Haidian District, Beijing, 100191, China

[d] Department of Electrical Engineering & Electronics, University of Liverpool, Brownlow Hill, Liverpool, L69 3GJ, United Kingdom

[*] Corresponding author.
Tel/Fax: +86-10-82338120
E-mail address: sunif@buaa.edu.cn

Abstract

Pyrolysis of pine sawdust, a typical industrial biomass waste, was studied. The effects of operating temperature, biomass particle size, and carrier gas space velocity on the products of biomass pyrolysis were investigated. A three-layer artificial neural network (ANN) model was developed and trained to simulate and predict the selectivity and yield of gas products. Good agreement was achieved between the experimental and simulated results. The major gas products of biomass pyrolysis are CO, CO_2, H_2, and CH_4. The ANN model showed that the major gas products depended mainly on the temperature, and the total selectivity of CO, CO_2, H_2, and CH_4 increased from 2.91% at 300℃ to 34.31% at 900℃. The selectivity of main gas products increased with increasing carrier gas flow rate. When the carrier gas flow rate increased from 45 min^{-1} to 85 min^{-1}, the selectivity of major gas products increased from 29.12% to 34.03%. Within the sample particle size range from 0.1 to 1.7 mm, there was no significant difference in the selectivity of major gas products. The pyrolysis temperature also influenced the composition of the tar in the biomass pyrolysis product. In the temperature range investigated, the benzene composition was favored at lower temperatures, such as 400℃, however, the light-weight PAHs were preferably generated at higher temperatures above 600℃.

Key words: pyrolysis; biomass; tar; artificial neural network (ANN); non-condensable gas

1. Introduction

Biomass pyrolysis is a type of thermolysis, thermochemical decomposition of organic material at elevated temperatures in the absence of oxygen, which produces tar, condensable liquid and non-condensable gas products. Biomass pyrolysis process is usually divided into four stages based on a thermal viewpoint [1,2]. In the drying stage in which the temperature is below 100℃, the biomass releases moisture and some bound water. In the initial stage, the biomass temperature is between 100 and 200℃. This releases low-molecular-weight gases, such as CO and CO_2, and small amounts of acetic acid. In the intermediate stage, the temperature is between 200 and 600℃. Most of the vapor or precursors to bio-oil are produced at this stage. Large molecules of biomass particles decompose into char, condensable gases, and non-condensable gases. The final stage takes place at a temperature between 300 and 900℃. The final stage of pyrolysis involves secondary cracking of volatiles into char and non-condensable gases. If they stay in the biomass long enough, large molecule condensable gases will also crack, producing additional char (secondary char) and gases. The condensable gases, if removed quickly from the reaction, condense outside in the downstream reactor as tar or bio-oil. A higher pyrolysis temperature also favors the production of hydrogen, which increases quickly above 600℃ [3].

Biomass pyrolysis produces non-condensable gases (including H_2, CO, CH_4, and CO_2) tar, and char [4]. Many factors, such as biomass particle diameter, temperature, heating rate, and residence time can influence the production rate and product properties of biomass pyrolysis [5]. Temperature is the most important factor.

Biomass releases different products under different temperature profiles [16-19]. Several researchers [20-23] have investigated the product selectivity and production rate of biomass pyrolysis at different temperatures, ranging from 300 to 1000 ℃, in a fluidized bed reactor or revolver. Biomass particle size is also an important factor affecting the pyrolysis reaction rate. Biomass particles with larger diameters have weaker heat transfer capacity, so the internal temperature increases slowly, which affects the selectivity of biomass pyrolysis. Researchers have investigated the relationship between biomass particle size and the selectivity of biomass pyrolysis in fluidized and free-fall reactors [5,24]. The results show that biomass with smaller particle diameters releases more gases, and less tar and char; the fraction of H_2 and CO will increase as the biomass particle diameter becomes even smaller. Cui [25] analyzed biomass pyrolysis via thermogravimetric analysis and a self-designed pressurized thermal gravitational analyzer and concluded that the reaction rate of biomass pyrolysis was higher under higher pressure. Generally, heating rate, flow rate, biomass molecular structure, and reactor pressure influence the composition of products from biomass pyrolysis.

Tar is a by-product of biomass pyrolysis, the composition of which is very complex. Currently, more than 300 compounds have been detected in tar; despite this, many compounds remain unknown [26,27]. Tar usually comprises mostly benzene derivatives and polycyclic aromatic hydrocarbons (PAHs) [28-32]. The fractions of six compounds in particular are typically each greater than 5%, including benzene, naphthalene, methylbenzene, ethenylbenzene, phenol, and indene. These compounds

are liquids at low temperatures and crack into permanent gases with low molecular weights at high temperatures. These small-molecule gases do not condense into liquids when the reactor temperature falls back to the range within which the original compounds are liquids. Recently, many researchers investigated the reactions of tar at different temperatures. Tar starts to condense below 200℃ and starts to react and produce char, pyroligneous acid, additional tar (secondary tar), and gases above 200℃. Above 600℃, the secondary tar and pyroligneous acid are evaporated and mixed, producing gases. At a temperature of 500℃, the production rate of tar from biomass pyrolysis is highest. Biomass pyrolysis produces tar through a series of complicated reactions. They depend on many reaction factors, but especially reaction temperature. Tar in the vapor phase cracks into light hydrocarbons, aromatic hydrocarbons, alkenes, hydrocarbons, and PAHs as the reactor temperature increases.

Chemical kinetic models are one approach to gain insight into a reaction and provide a better understanding of the effect of the processing parameters. The kinetic models reported by Di Blasi [33] is a typical example that investigated the influence of several variables for wood and biomass pyrolysis, such as reaction temperature, residence time, and pressure. Although a dynamic model provides relatively stable and accurate performance in this reaction, a complicated structure is required, especially for a multiple responses system/multi-stage reaction process which contains many processing parameters and mechanisms.

Compared with ‘traditional’ chemical and physical models, artificial neural networks have the advantages of being able to model complex phenomena rapidly and

easily by simply starting with measured values and investigating potentially complex and non-linear relationships, linking various physical values. Additionally, a neural network has versatility as a black box information processor. All fields including neural network applications use the same symbols. Regardless of the form, neurons represent the same ingredient in different neural networks. This commonality makes it possible to share the same neural network theory and algorithms across various areas. Mikulandric et al [34] compared the effects of equilibrium models and neural network model in the biomass gasification process in fixed bed gasifiers. The results derived from different equilibrium modelling approaches (for various operating conditions) cannot be compared or explained in some cases. Results from devised equilibrium models are comparable with results derived from literature only for specific operating points. However, neural network models showed good capability to predict biomass gasification process parameters with reasonable accuracy and speed. As a consequence, the effective utilization of the ANN model was beneficial in understanding the complex relationship between the raw materials and pyrolysis products and even the technical management in the actual pyrolysis process [35].

In this study, the distribution of biomass pyrolysis products and the effects of operation conditions on pyrolysis were investigated. We summarized rules on the influences of temperature, biomass particle size, and carrier gas space velocity on biomass pyrolysis products. Moreover, an ANN model was developed and trained to simulate and predict the selectivity and yields of gas products with different operation parameters in the biomass pyrolysis.

2. Materials and Methods

2.1 Raw material

The typical biomass selected for pyrolysis was pine sawdust (without bark, purchased from Porta Pine, Germany). This biomass was milled, sieved, and classified to obtain fractions of uniform particle size, and then dried for at least 12 h at 105℃. The particle size of the biomass was classified into six groups: 0.14, 0.17, 0.22, 0.34, 0.64, and 1.70 mm. Nitrogen (99.999 vol.%, Beijing Haipu Gas Co. Ltd., China) was used as the carrier gas. Analytical-grade methanol (Beijing Chemical Works, China) was used as the tar absorbent.

2.2 Experimental setup

The configuration of the pyrolysis reactor is shown in Fig. 1. The pyrolysis apparatus consists of a quartz tubular reactor (Length: 1 m and the inner diameter: 50 mm). The reactor is heated by a tube furnace (OTF-1200X, Hefei Kejing Material Technology Co. Ltd., China) in an inert N_2 atmosphere. First, 4 g of pine sawdust was introduced into the furnace. The flow rate of carrier gas (N_2) was controlled by a mass flow controller (D08-4E, Beijing Seven Star Electronics Co. Ltd., China). For each experimental run, the reactor was heated to a set temperature (400, 500, 600, 700, or 800℃) at a heating rate of 20℃ min^{-1} prior to pushing the biomass sample into the heated zone. The reaction time was 30 min. The volatile products passed through two impingers filled with methanol which were cooled in ice-water bath, and the produced tar was remained in the impingers. The remaining aerosol was removed with a filter

142 filled with degreasing cotton. The gas product passed through a wet type gas
143 flowmeter to record the total gas volume. Finally, the gas product was collected in a
144 sampling gas bag (15 L, Dalian Delin Gas Packaging Co. Ltd., China).

145 **2.3 Analytical methods**

146 Produced gases were analyzed by a GC-17A (Shimadzu Corp., Japan) equipped
147 with a thermal conductivity detector (TCD) and a Carboxen-1010 PLOT capillary
148 column (30 m × 0.53-mm I.D., 30-μm average thicknesses, Supelco Corp., USA). The
149 injection (injection volume of 200 μL) was performed at 100℃ in splitless mode. The
150 oven temperature program was 50℃ constantly for 15 min. The temperature of the
151 detector was 200℃. Argon (99.999 vol.%, Beijing Haipu Gas Co. Ltd., China) was
152 used as the carrier gas, at a constant flow of 10 mL/min.

153 TG analysis was carried out with a STA449F3 Jupiter (Netzsch-Gerätebau
154 GmbH, Germany). Approximately 40 mg of pine sawdust were heated in argon at
155 10℃ min^{-1}, from ambient to 800℃ for pyrolysis.

156 The yield and selectivity of gas product were calculated as follows:

157 The yield of gas product (mmol/g) = $\frac{V_o}{24.4\times4}$ (1)

158 The selectivity of gas product (%) = $\frac{c_j}{c}$ × 100% (2)

159 The molar ratio of gas products (mol%) = $\frac{n_j}{n}$ × 100% (3)

160 where v_o is the volume of gas product from pyrolysis of 4 g pine sawdust at room
161 temperature (25℃), c_j is the mass of target gas product (g), c is the mass of pine
162 sawdust used in the biomass pyrolysis (g), n_j is the molar quantity of target gas
163 product (mol), j is different kind of gas products, and n is the molar quantity of total

gas products produced in the biomass pyrolysis (mol). All experiments were conducted three times under the same experimental conditions.

2.4 Tar sampling

The products in the pyrolysis process flowed through two impingers filled with 100 mL methanol. The solvents in the impingers were passed through an organic filter membrane to remove solid particles and were then diluted with methanol. A 3D-fluorescence spectrophotometer (F-7000, Hitachi Corporation, Japan) with a 1 cm light-path length was used to record the 3D-fluorescence spectra of the tar. The scan speed was 12000 nm/min, the PMT voltage was 700 V, and the response time was 0.002 s.

2.5 Artificial neural network

An artificial neural network is a layer-parallel information processing structure composed of numerous neurons connected by weighted links, passing signals from one neuron to another. A typical neural network consists of multiple layers, including an input layer, a number of hidden layers, and an output layer. The input layer is a terminal to receive and distribute the input information, while the output layer is the final product of the neural processing. Between the input and output layers are one or more hidden layers, which build up the links between the inputs and outputs. In this paper, a three-layer back propagation (BP) neural network with a logarithm sigmoid function in the hidden layer and a linear function at the output layer was used for the training of the neural network.

The experimental data were split into two groups: input set (X) and target output set (T). Three processing parameters, space velocity, reaction temperature, and particle size, were identified as input variables in the model, while the target output variables include selectivity of the four gas products (H_2, CO, CH_4, CO_2). The selectivity for the gas products of the pyrolysis processing can be calculated from the simulated output variables. Additionally, the experimental data were divided randomly into training and test data sets. The training step was used to determine the connection weights between layers, while the test step was used to evaluate the accuracy of the model.

3. Results and Discussion

3.1 Neural network modeling

3.1.1 Selection of back-propagation training algorithm

The most widely used neural network architecture is back-propagation (BP), which is a hierarchical design consisting of entirely cross-linked layers. A valid neural network with accompanying proper and fixed weights is achieved when the mean square error (MSE) of the test set reaches a minimum value. In our recent work, we have trained a three-layer feed-forward neural network with different BP algorithms. The Levenberg-Marquardt (LM) training algorithm has shown excellent performance in prediction and function approximation with a minimum MSE value achieved compared with other BP algorithms, consistent with other studies. In this study, the LM algorithm was combined with seven different transfer functions to get the optimal

neural network system that could provide a stable and accurate prediction for the biomass pyrolysis process.

3.1.2 Optimization of neuron number

In this work, the LM training algorithm with a logarithmic sigmoid transfer function at the hidden layer and a linear transfer function at the output layer was used for training of the BP neural network (Fig. 2). The optimal number of neurons in the hidden layer is determined based on the minimum value of MSE for the training and test sets. We found the MSE and SED values for four neurons were 0.070389 and 0.064, respectively, with four neurons in the hidden layer. Both values decreased significantly, to 0.01 and 0.04, respectively, when seven neurons were used. However, further increasing the number of neuron to 12 did not reduce the MSE or SED significantly. Thus, the optimal neuron number in the hidden layer for the LM-BP structure was determined to be seven.

3.1.3 Testing the neural network model

A test group that included about 15% of the experimental data was used to feed the optimized ANN to evaluate the accuracy of the model. Fig. 3 shows a comparison between the experimental data and those predicted from the LM-BP neural network model. Two lines can be seen in the figure: one is the perfect fit line, Y = T. Here, Y is the predicted result and T the experimental, meaning the predicted results were essentially identical to the actual input results.

3.1.4 Sensitivity analysis

The neural net weight matrix and Garson equation were used to determine the relative importance of the input plasma processing parameters. This equation is based on the partitioning of connection weights of the optimal ANN model:

$$I_j = \frac{\sum_{m=1}^{m=N_h} \left(\left(\left| W_{jm}^{ih} \right| \Big/ \sum_{k=1}^{N_i} \left| W_{km}^{ih} \right| \right) \times \left| W_{mn}^{ho} \right| \right)}{\sum_{k=1}^{k=N_i} \left\{ \sum_{m=1}^{m=N_h} \left(\left| W_{km}^{ih} \right| \Big/ \sum_{k=1}^{N_i} \left| W_{km}^{ih} \right| \right) \times \left| W_{mn}^{ho} \right| \right\}} \quad (4)$$

where I_j is the relative importance of the j^{th} input variable for the whole process, N_i and N_h are the number of input and hidden neurons, respectively. W represents the connection weight. Additionally, the superscripts 'i,' 'h,' and 'o' refer to the input, hidden, and output layers, respectively, while the subscripts 'k,' 'm,' and 'n' refer to the input, hidden, and output neurons.

Table 1 presents the weights produced by the optimized ANN that were used in this work. The relative importance of the input parameters was determined by Eq. 1, as shown in Table 2. In this study, temperature had a significant impact on the reaction performance of the pyrolysis process in terms of the selectivity of gas product (H_2, CO, CH_4, and CO_2). Particle size was identified as a second important parameter on the CO and H_2 selectivity. In contrast, the space velocity contributed least to the pyrolysis process, because of its lowest importance for all outputs.

Table 1. Weight matrices W_1 (weights between input and hidden layer) and W_2 (weights between hidden and output layers).

	W_1			W_2
Neuron	Input variables			Outputs (%)
	Space	Temperature	Particle	Selectivity

	Velocity		Size	H_2	CO	CH_4	CO_2
1	0.539	3.041	-0.841	0.756	1.292	1.257	0.442
2	0.763	10.186	2.694	1.294	0.792	0.753	1.549
3	0.878	2.501	-2.025	-0.539	-0.331	-0.478	-0.037

Table 2. Relative importance of processing parameters for the optimized ANN model.

Input variable	Importance (%)			
	Selectivity			
	H_2	CO	CH_4	CO_2
Space Velocity	19.18	19.77	19.54	19.50
Temperature	60.85	58.11	57.52	63.51
Particle Size	19.97	22.12	22.94	16.99
Total	100	100	100	100

3.2 Effect of temperature on pyrolysis products

The effect of pyrolysis temperature on gas products is shown in Fig. 4. Under these operating conditions, the space velocity was 65 min^{-1}, and the biomass particle size was 0.14-1.70 mm. At the highest temperature in the investigation range (800℃), the yield of total gas product reached a maximum of about 30.6 mmol/g (RSD = 1.6%), while at 400℃ it was 6.8 mmol/g (RSD = 6.9%). The main gas products from the pyrolysis of biomass are H_2, CO, CH_4, and CO_2.

Fig. 5 shows a comparison between the predicted and experimental results for the selectivities of H_2, CO, CH_4, and CO_2 at different temperatures. The simulated data obtained from the well-trained neural network model were in fairly good agreement

with the experimental data. Temperature showed a significant impact on the pyrolysis reaction performance. With an increase of temperature from 400℃ to 800℃, the selectivity of H_2 increased from 0.04% to 5.89%, CO from 0.52% to 15.20% and CH_4 from 0.20% to 5.78%, CO_2 from 2.15% to 6.21% (RSD is between 7.6% and 1.3%). The reactor temperature influences the pyrolysis process, which determines the gas product distribution. The molar ratio of major gas products in the total gas products increased from 46.11 mol% to 80.11 mol% with temperature increasing from 400 to 800℃.

Higher temperature favors the cracking and reforming of hydrocarbons and thus increases H_2 and CO formation. With the temperature increase from 400 to 800℃, the yield of H_2 increased from 0.33 to 17.41 mmol/g and CO from 0.68 to 12.99 mmol/g. As shown in Table 3, the total ratio of H_2 and CO in the gas products, defined as syngas, reached 56.71% at 800℃. Over the investigated temperature range, the higher temperature contributed to higher H_2 and CO selectivity. The H_2/CO molar ratio also increased from 0.12 to 0.34 mol/mol as the pyrolysis temperature rose from 400 to 800℃.

Table 3. Effect of temperature on the total ratio of H_2 and CO and molar ratio of H_2 to CO in gaseous product from pyrolysis (sample particle size: 0.45–0.90 mm; space velocity: 65 min^{-1}).

Temperature (℃)	400	500	600	700	800
H_2+CO (%) [a]	11.24	16.35	29.63	44.99	56.71
H_2/CO (mol/mol) [b]	0.12	0.08	0.16	0.27	0.34

[a] *The total ratio of H_2 and CO among the total gas products, $(n_{H_2} + n_{CO})/n$.*

[b] *The molar ratio of H_2 to CO in the gas products,n_{H_2}/n_{CO}.*

The gas product distribution was influenced by the composition of the biomass and the properties of its components. In the pyrolysis process, the gas products originated from the primary pyrolysis and were also products of the secondary decomposition of volatiles. The CO was from unstable carbonyls in the volatiles [36]. Because CO originated mainly from the secondary decomposition of volatiles cracked by primary pyrolysis, the selectivity of CO obviously increased with increased temperature. The H_2 resulted mainly from the rearrangement and dehydrogenation of aromatic bonds. As a result, the selectivity of H_2 also obviously increased with increasing temperature from 400 to 800℃.

The formation of CO_2 was mainly the result of the primary decomposition of alduronic acid in hemicelluloses at low temperature, about 350℃ [37]. When the temperature increased, the carboxyls in the lignin broke up and produced a small quantity of CO_2. For this reason, with temperature increased, the ratio of CO_2 in the gas products decreased but the selectivity increased. The product of CH_4 was formed by the decomposition of methoxyl in lignin. The higher temperature promoted lignin decomposition and the selectivity of CH_4 increased, from 3.82 to 13.10%.

The generated tar in biomass pyrolysis was analyzed by the 3-D fluorescence spectrophotometer. When the fluorescence peak of Ex/Em is near the 270/335 nm point (Peak A in Fig. 6), the peak is related to the 1- or 2-ring aromatics in solution: mostly benzene, toluene, and phenol [38]. It can be concluded from Table 4 that with temperature increasing from 400 to 600℃, the peak intensity of the benzene

300 composition from biomass pyrolysis decreased, from 3062 to 1194, and then
301 maintained a stable lower level when the temperature increased above 600-700℃. In
302 the temperature range investigated, the benzene composition was favored at lower
303 temperatures, such as 400℃ and it will decompose at higher temperatures. It can be
304 concluded that higher temperatures promote the formation of gaseous products at the
305 expense of tar. Moreover, with the temperature increasing above 600℃, there was
306 another fluorescence peak of Ex/Em near 230/355 nm, which was related to the 2- or
307 3-ring polycyclic aromatic hydrocarbons (PAHs). The value of peak B increased from
308 1148 to 1174 with pyrolysis temperature increasing from 600 to 800℃. It can be
309 concluded that light-weight PAHs were preferably generated at higher temperatures,
310 above 600℃ [39]. Also, at very high temperatures (> 600-700℃),
311 dehydrogenation/aromatization reactions can lead to formation of polynuclear
312 aromatic hydrocarbons and, eventually, increase carbonization.

313 Table 4. The intensity of peaks from 3D fluorescence scan on tars of pyrolysis.

Temperature/℃	400	500	600	700	800
Peak A Intensity	3062	2250	1194	1287	1107
Peak B Intensity	No peak	No peak	1148	1653	1774

314

315 **3.3 Effect of carrier gas space velocity on pyrolysis gaseous products**

316 The space velocity of the carrier gas N_2 was set at 45, 65, and 85 min^{-1}. As
317 shown in Fig. 7, while the space velocity (in standard conditions, the volume of gas
318 crossing the reactor in unit time) increased from 45 to 85 min^{-1}, the total ratio of major

gaseous products, including H_2, CO, CH_4, and CO_2, among the total gas products increased from 85.19 to 89.4 mol%. As seen in Fig. 8, a near-perfect match between the experimental and simulated data at different space velocities was achieved. The selectivity of H_2 increased from 5.19 to 6.10%, CO from 13.36 to 15.86%, and CH_4 from 4.81 to 5.72%, whereas CO_2 from 5.76 to 6.34% (RSD was 2.0-7.0%), with the space velocity increase from 45 to 85 min^{-1}. Primary decomposition of biomass material (< 400℃) consists of a degradation process, whereas secondary thermolysis (> 400℃) involves aromatization processes [40]. The primary pyrolysis products inside and around the biomass particles in the gas phase will react in secondary pyrolysis. Secondary pyrolysis can produce permanent gases, such as H_2, CH_4, CO and CO_2. In this investigation, increasing the space velocity would remove the primary pyrolysis products attached to the biomass particles faster, which may otherwise hinder the biomass pyrolysis. Thus, secondary pyrolysis reactions would be promoted. As a consequence, more permanent gases was produced.

3.4 Effect of biomass sample particle size on pyrolysis gaseous products

The effect of particle size on the total yield and ratios of gas products are shown in Fig. 9. The total yield of main gas products increased from 30.7 to 32.5 mmol/g-biomass with a decrease in particle size (from 1.400-2.000 to 0.150-0.180 mm). However, the selectivity of H_2, CO, CH_4, and CO_2 was almost not influenced by the particle size (RSD was between 1.3% and 10%). As a consequence, the reaction mechanism was almost unaffected by particle size. Additionally, the prediction results of the selectivity of CO_2, H_2, CH_4 and CO were in good agreement with the

experimental data with different particle sizes in pyrolysis process (shown in Fig. 10), indicating the good potential of the ANN model in simulating the complex pyrolysis process of biomass.

Typical TG, DSC and DTG curves for biomass are shown in Fig. 11. When the temperature was lower than 200℃, the DSC curves showed an endothermic peak around 100℃, mainly attributable to dehydration of biomass. In the temperature range of 200-500℃, a DTG peak and sharp decrease in the TG curve are seen. There is an obvious peak around 360℃ and then an inconspicuous peak at around 310℃ in the DTG curve. The DSC curve also shows an obvious endothermic peak at around 360℃. This is mainly relevant to the composition of the biomass. Biomass is typically composed of cellulose, hemicellulose, and lignin [41]. Under 'ordinary' heating, cellulose pyrolysis occurs around 250-500℃, hemicellulose pyrolysis at below 350℃, and lignin pyrolysis over the whole temperature rang from ambient to 900℃, but at a slow mass loss rate [42]. The weight loss peaks of hemicellulose and cellulose partially overlap each other. However, the lignin has no sharp weight loss peak.

With an increase in particle size from 0.150-0.180 to 1.400-2.000 mm, the TG curves and product gas composition were almost not influenced by particle size. The main reason is that the difference in the particle size was small, from 0.150-0.180 to 1.400-2.000 mm. As seen in Fig. 11 (b), the amount of carbon residue increased from 20.38 to 21.26 wt.%, with particle size decreasing from 1.400-2.000 to 0.150-0.180 mm. The main reason is that the smaller particles can decompose more completely, leave less char and achieve more complete energy conversion.

4. Conclusions

In this work, effects of operating temperature, carrier gas space velocity, and biomass particle size on characteristics of biomass pyrolysis were investigated. A three-layer BP neural network was developed to simulate and predict the complex biomass pyrolysis process. The LM training algorithm combined with a target sigmoid transfer function (logarithmic) in the hidden layer with seven neurons and a linear transfer function at the output layer offered the optimal solution for training the BP neural network. There was fairly good agreement between the experimental results and simulated data for the biomass pyrolysis process. The main gas products of biomass pyrolysis were CO, CO_2, H_2, and CH_4. The yields of the major gas products increased and the composition of the gas products changed as temperature increasing. The tar composition was also influenced by temperature. The benzene composition was favored at lower temperatures, such as 400℃, whereas, the PAHs tended to generate at higher temperature of over 600℃. With the carrier gas space velocity increasing, selectivity of the major products also increased. A large space velocity of carrier gas was beneficial for syngas production. The characteristics of biomass pyrolysis were almost not influenced by the biomass particle size.

5. Acknowledgements

The authors are grateful to National Natural Science Foundation of China (Project No. 21477006) for providing financial assistances.

Figure captions:

Fig. 1. The schematic of the biomass pyrolysis reactor.

Fig. 2. Optimized three-layer ANN model with a logarithm sigmoid transfer function at the hidden layer and a linear function at the output layer.

Fig. 3. Comparison between the experimental data (target output) and predicted output data for the optimized ANN.

Fig. 4. Effect of pyrolysis temperature on the yield of gas products.

Fig. 5. Comparison between the experimental data (target output) and predicted output data of the selectivity of CO_2 (a), H_2 (b), CH_4 and CO (d) at different operating temperatures in pyrolysis process. (Space velocity: 65 min^{-1}; particle size: 0.6375 mm)

Fig. 6. 3D fluorescence spectra on tar from pyrolysis of biomass at different temperatures: (a) 400℃, (b) 500℃, (c) 600℃, (d) 700℃ and (e) 800℃

Fig. 7. Effect of carrier gas flow rate on gas product from pyrolysis of biomass.

Fig. 8. Effect of space velocity on the selectivity of gas products (Temperature: 800℃; particle size: 0.6375 mm) and comparison of predicted and experimental results.

Fig. 9. Effect of sample particle size on yield of gas products (a) and composition of gas products (b) in the biomass pyrolysis process.

Fig. 10. Comparison between the experimental data (target output) and predicted output data of the selectivity of CO_2 (a), H_2 (b), CH_4 and CO (d) with different particle sizes in pyrolysis process. (Space velocity: 65 min^{-1}; Temperature: 800 ^oC)

405 Fig. 11. DTG, DSC (a) and TG (b) curves of biomass for different particle sizes
406 (1.400~2.000 mm; 0.425~0.850 mm and 0.150~0.180 mm) at heating rate of
407 10℃/min.

408

409 **References**

410 [1] Y. Lin, G. Huber, The critical role of heterogeneous catalysis in lignocellulosic
411 biomass conversion, Energy Environ. Sci. 2 (2009) 68-80.

412 [2] M. Van de Velden, J. Baeyens, A. Brems, B. Janssens, R. Dewil, Fundamentals,
413 kinetics and endothermicity of the biomass pyrolysis reaction, Renew. Energy 35
414 (2010) 232-242.

415 [3] C. Z. Wu, Modern utilization technology of biomass energy, Chemical Industry
416 Press, Beijing, 2003. (in Chinese)

417 [4] J. E. White, W. J. Catallo, B. L. Legendre, Biomass pyrolysis kinetics: a
418 comparative critical review with relevant agricultural residue case studies, J. Anal.
419 Appl. Pyrolysis 91 **(**2011) 1-33.

420 [5] Q. Lu, W. Li, X. Zhu, Overview of fuel properties of biomass fast pyrolysis oils,
421 Energy Convers. Manag. 50 (2009) 1376-1383.

422 [6] F. Karaosmanoğlu, E. Tetik, E. Göllü, Biofuel production using slow pyrolysis of
423 the straw and stalk of the rapeseed plant, Fuel Process. Technol. 59 (1999) 1-12.

424 [7] S. Şensöz, Slow pyrolysis of wood barks from Pinus brutia Ten. and product
425 compositions, Bioresour. Technol. 89 (2003) 307-311.

426 [8] O. Onay, O. M. Kockar, Slow, fast and flash pyrolysis of rapeseed, Renew. Energy
427 28 (2003) 2417-2433.
428 [9] A. E. Pütün, E. Ö nal, B. B. Uzun and N. Ö zbay, Comparison between the “slow”
429 and “fast” pyrolysis of tobacco residue, Ind. Crops Prod.26 (2007) 307-314.
430 [10] V. Kirubakaran, V. Sivaramakrishnan, R. Nalini, T. Sekar, M. Premalatha, P.
431 Subramanian, A review on gasification of biomass, Renew. Sustainable Energy Rev.
432 13 (2009) 179-186.
433 [11] D. Meier, O. Faix, State of the art of applied fast pyrolysis of lignocellulosic
434 materials-a review, Bioresour. Technol. 68 (1999) 71-77.
435 [12] J. Yanik, C. Kornmayer, M. Saglam, M. Yüksel, Fast pyrolysis of agricultural
436 wastes: Characterization of pyrolysis products, Fuel Process. Technol. 88 (2007)
437 942-947.
438 [13] A. V. Bridgwater, Review of fast pyrolysis of biomass and product upgrading,
439 Biomass Bioenergy, 38 (2012) 68-94.
440 [14] D. S. Scott, J. Piskorz, D. Radlein, Liquid products from the continuous flash
441 pyrolysis of biomass, Ind. Eng. Chem. Res. Process Des. Development 24 (1985)
442 581-588.
443 [15] K. Sipilä, E. Kuoppala, L. Fagernäs, A. Oasmaa, Characterization of
444 biomass-based flash pyrolysis oils, Biomass Bioenergy 14 (1998) 103-113.
445 [16] R. Yan, H. Yang, T. Chin, D. T. Liang, H. Chen, C. Zheng, Influence of
446 temperature on the distribution of gaseous products from pyrolyzing palm oil wastes,
447 *Combust. Flame*, 142 (2005) 24-32.

448 [17] M. Phanphanich, S. Mani, Impact of torrefaction on the grindability and fuel
449 characteristics of forest biomass, Bioresour. Technol. 102 (2011) 1246-1253.
450 [18] E. Apaydın-Varol, A. E. Pütün, Preparation and characterization of pyrolytic
451 chars from different biomass sample, J. Anal. Appl. Pyrolysis 98 (2012) 29-36.
452 [19] M. Shoja, M. A. Babatabar, A. Tavasoli, A. Ataei, Production of hydrogen and
453 syngas via pyrolysis of bagasse in a dual bed reactor, J. Energy Chem. 22 (2013)
454 639-644.
455 [20] A. Li, X. Li, S. Li, Y. Ren, Y. Chi, J. Yan, K. Cen, Pyrolysis of solid waste in a
456 rotary kiln: influence of final pyrolysis temperature on the pyrolysis products, J. Anal.
457 Appl. Pyrolysis 50 (1999) 149-162.
458 [21] T. R. Carlson, Y. T. Cheng, J. Jae, G. W. Huber, Production of green aromatics
459 and olefins by catalytic fast pyrolysis of wood sawdust, Energy Environ. Sci. 4 (2011)
460 145-161.
461 [22] Q. Bu, H. Lei, S. Ren, L. Wang, Q. Zhang, J. Tang, R. Ruan, Production of
462 phenols and biofuels by catalytic microwave pyrolysis of lignocellulosic biomass,
463 Bioresour. Technol. 108 (2012) 274-279.
464 [23] Y. Zhao, Y. Fu, Q. X. Guo, Production of aromatic hydrocarbons through
465 catalytic pyrolysis of γ-valerolactone from biomass, Bioresour. Technol. 114 (2012)
466 740-744.
467 [24] S. Luo, B. Xiao, Z. Hu, S. Liu, Effect of particle size on pyrolysis of
468 single-component municipal solid waste in fixed bed reactor, Int. J. Hydrog. Energy
469 35 (2010) 93-97.

[25] Y. B. Cui, X. P. Chen, L. F. Gu, Thermogravimetry research of the biomass pyrolysis properties under the normal pressures and boost pressures, Boiler Technol, . 35 (2004) 12-15. (in Chinese)

[26] A. Demirbas, The influence of temperature on the yields of compounds existing in bio-oils obtained from biomass samples via pyrolysis, Fuel Process. Technol. 88 (2007) 591-597.

[27] C. Li and K. Suzuki, Resources, properties and utilization of tar, Conservation Recycling 54 (2010) 905-915.

[28] P. H. Blanco, C. Wu, J. A. Onwudili, P. T. Williams, Characterization of tar from the pyrolysis/gasification of refuse derived fuel: influence of process parameters and catalysis, Energy Fuels 26 (2012) 2107-2115.

[29] A. Dufour, P. Girods, E. Masson, S. Normand, Y. Rogaume, A. Zoulalian, Comparison of two methods of measuring wood pyrolysis tar, J. Chromatogr. A 1164 (2007) 240-247.

[30] V. Nemanova, T. Nordgreen, K. Engvall, K. Sjöström, Biomass gasification in an atmospheric fluidised bed: tar reduction with experimental iron-based granules from Höganäs AB, Sweden, Catal. Today 176 (2011) 253-257.

[31] T. Phuphuakrat, T. Namioka, K. Yoshikawa, Tar removal from biomass pyrolysis gas in two-step function of decomposition and adsorption, Appl. Energy 87 (2010) 2203-2211.

[32] Y. Zhang, S. Kajitani, M. Ashizawa, Y. Oki, Tar destruction and coke formation during rapid pyrolysis and gasification of biomass in a drop-tube furnace, Fuel 89

492 (2010) 302-309.
493 [33] C. Di Blasi, Modeling chemical and physical processes of wood and biomass
494 pyrolysis, Prog. Energy Combus. Sci. 34 (2008) 47-90.
495 [34] R. Mikulandrić, D. Lončar, D. Böhning, R. Böhme, M. Beckmann, Artificial
496 neural network modelling approach for a biomass gasification process in fixed bed
497 gasifiers, Energy Convers. Manag. 87 (2014) 1210-1223.
498 [35] M. A. Serio, Y. Chen, M. A. Wojtowicz, E. M. Suuberg, Pyrolysis processing for
499 solid waste resource recovery in space, In 30th International Conference on
500 Environmental Systems, (2000), Toulouse, France.
501 [36] E. Avni, R. W. Coughlin, P. R. Solomon, H. H. King, Mathematical modelling of
502 lignin pyrolysis, Fuel 64 (1985) 1495-1501.
503 [37] W. P. Pan, G. N. Richards, Influence of metal ions on volatile products of
504 pyrolysis of wood, J. Anal. Appl. Pyrolysis 16 (1989) 117-126.
505 [38] Z. Zhou, Z. Liu, L. Guo, Chemical evolution of Macondo crude oil during
506 laboratory degradation as characterized by fluorescence EEMs and hydrocarbon
507 composition, Mar. Pollut. Bull. 66 (2013) 164-175.
508 [39] D. Mohan, C. U. Pittman, P. H. Steele, Pyrolysis of wood/biomass for bio-oil: a
509 critical review, Energy Fuels 20 (2006) 848-889.
510 [40] S. Yaman, Pyrolysis of biomass to produce fuels and chemical feedstocks, Energy
511 Convers. Manag. 45 (2004) 651-671.
512 [41] S. Li, S. Xu, S. Liu, C. Yang, Q. Lu, Fast pyrolysis of biomass in free-fall reactor
513 for hydrogen-rich gas, Fuel Process. Technol. 85 (2004) 1201-1211.

[42] H. Yang, R. Yan, H. Chen, D. H. Lee, C. Zheng, Characteristics of hemicellulose, cellulose and lignin pyrolysis, Fuel 86 (2007) 1781-1788.

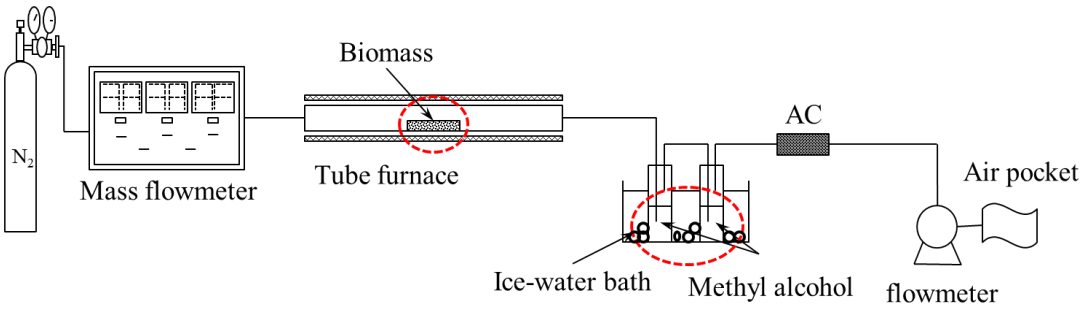

536

537 Fig. 1. The schematic of the biomass pyrolysis reactor

538

539

540

541

542

543

544

545

546

547

548

549

550

551

552

553

554

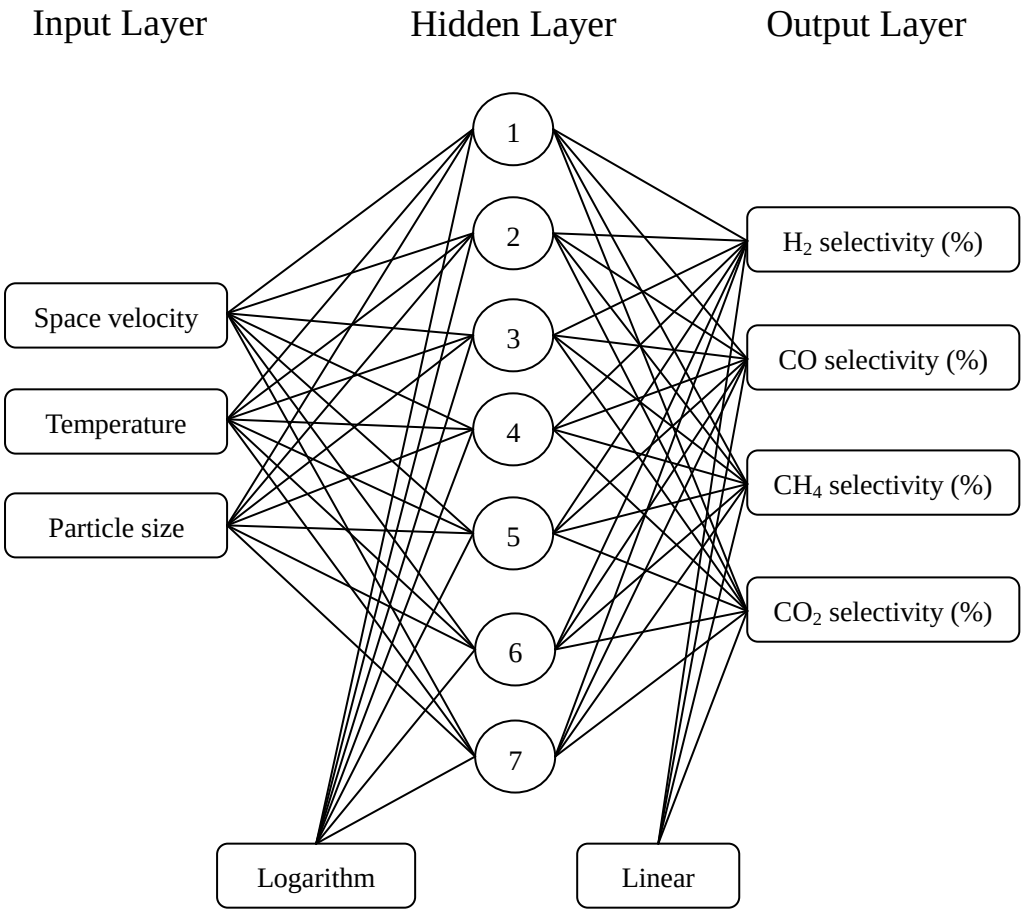

Fig. 2. Optimized three-layer ANN model with a logarithm sigmoid transfer function at the hidden layer and a linear function at the output layer.

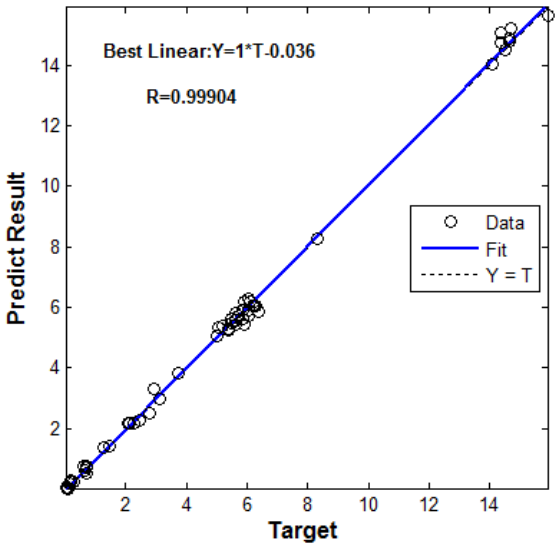

Fig. 3. Comparison between the experimental data (target output) and predicted output data for the optimized ANN.

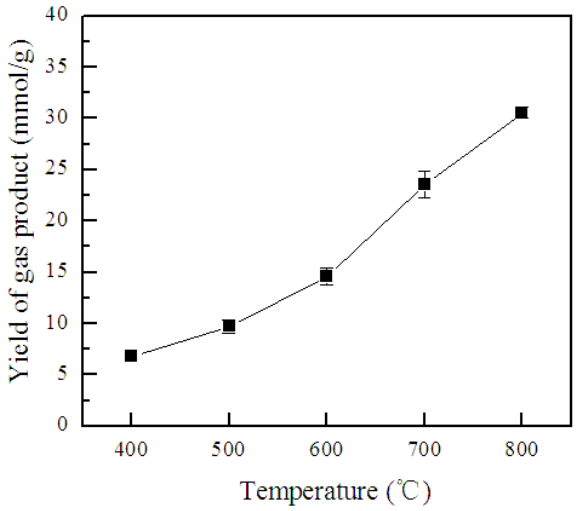

582

583 Fig. 4. Effect of pyrolysis temperature on the yield of gas products.

584

585

586

587

588

589

590

591

592

593

594

595

596

597

598

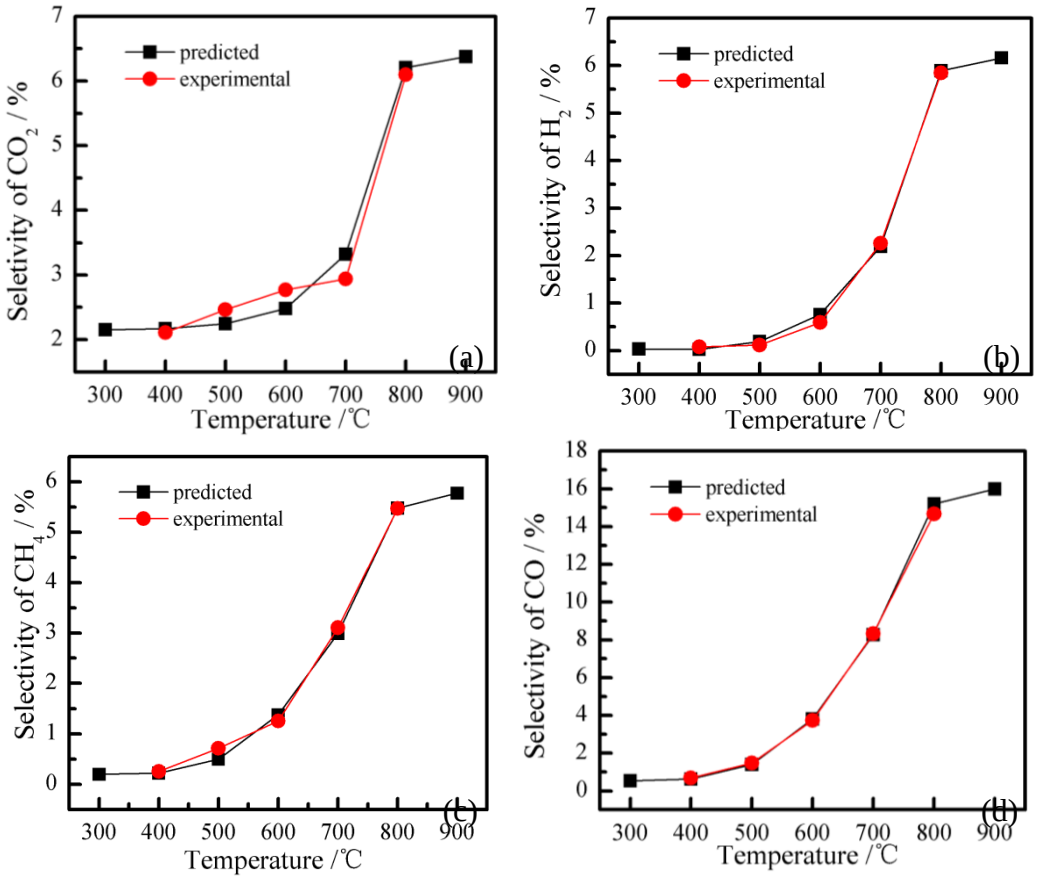

Fig. 5. Comparison between the experimental data (target output) and predicted output data of the selectivity of CO_2 (a), H_2 (b), CH_4 and CO (d) at different operating temperatures in pyrolysis process. (Space velocity: 65 min^{-1}; particle size: 0.6375 mm)

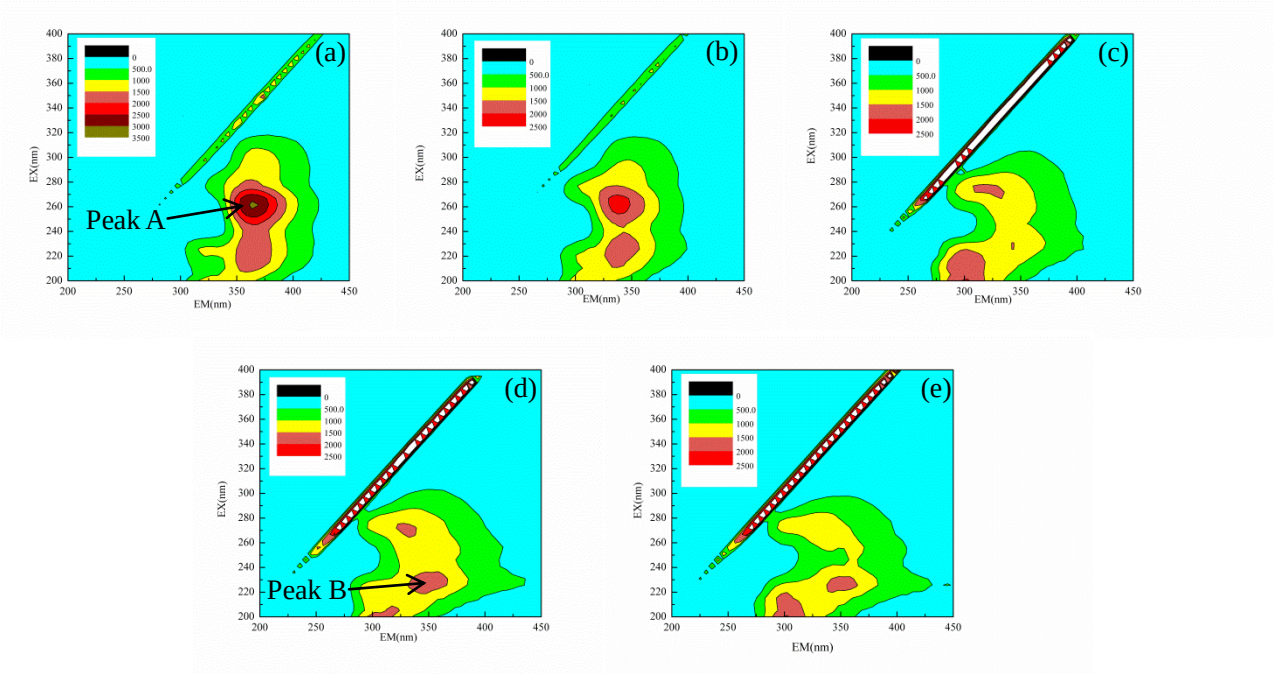

Fig. 6. 3D fluorescence spectra o n tar from pyrolysis of biomass at different temperatures: (a) 400℃, (b) 500℃, (c) 600℃, (d) 700℃ and (e) 800℃

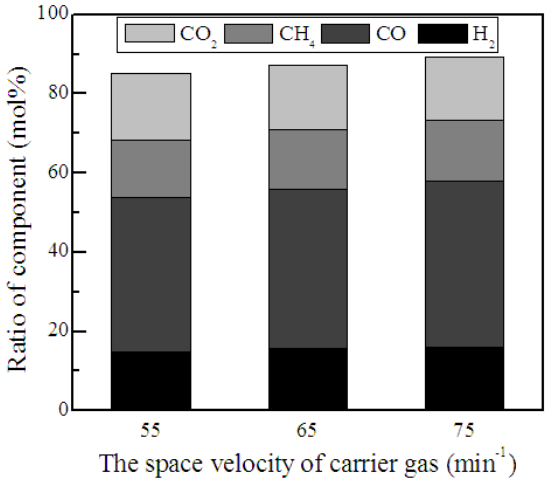

Fig. 7. Effect of carrier gas flow rate on gas product from pyrolysis of biomass.

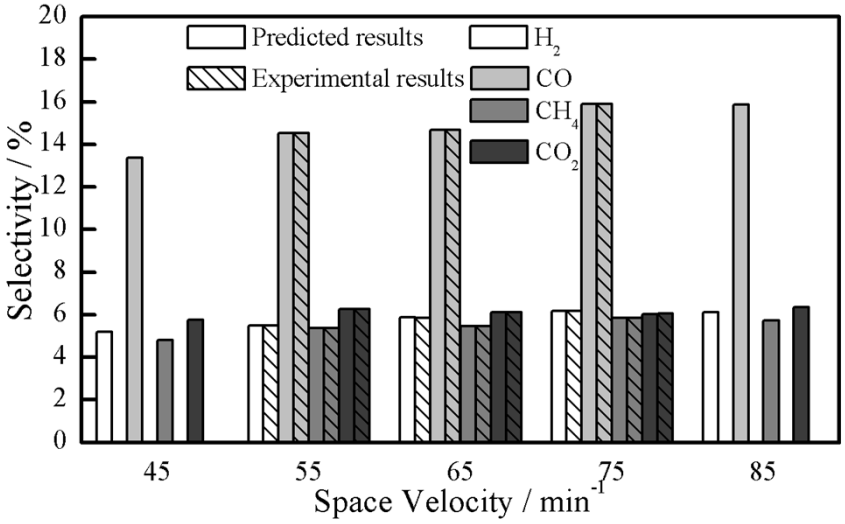

Fig. 8. Effect of space velocity on the selectivity of gas products (Temperature: 800℃; particle size: 0.6375 mm) and comparison of predicted and experimental results

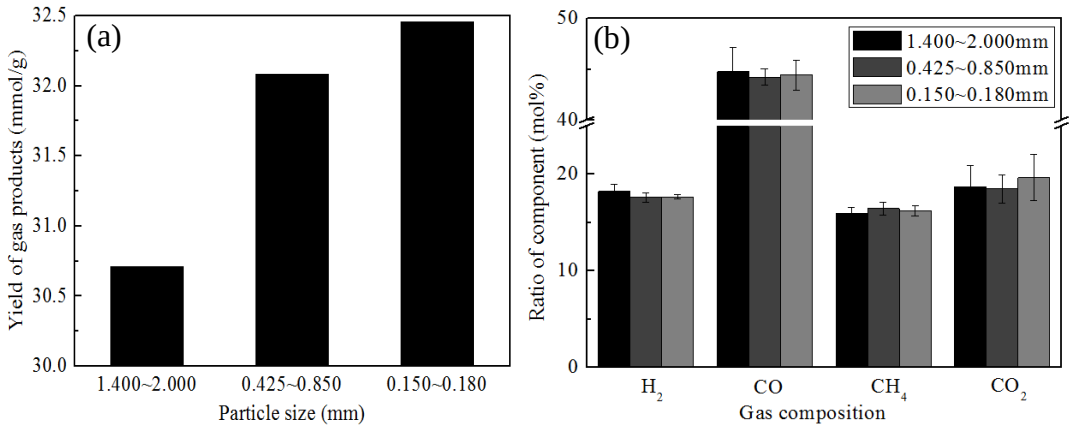

669

670 Fig. 9. Effect of sample particle size on yield of gas products (a) and composition of

671 gas products (b) in the biomass pyrolysis process.

672

673

674

675

676

677

678

679

680

681

682

683

684

685

686

687

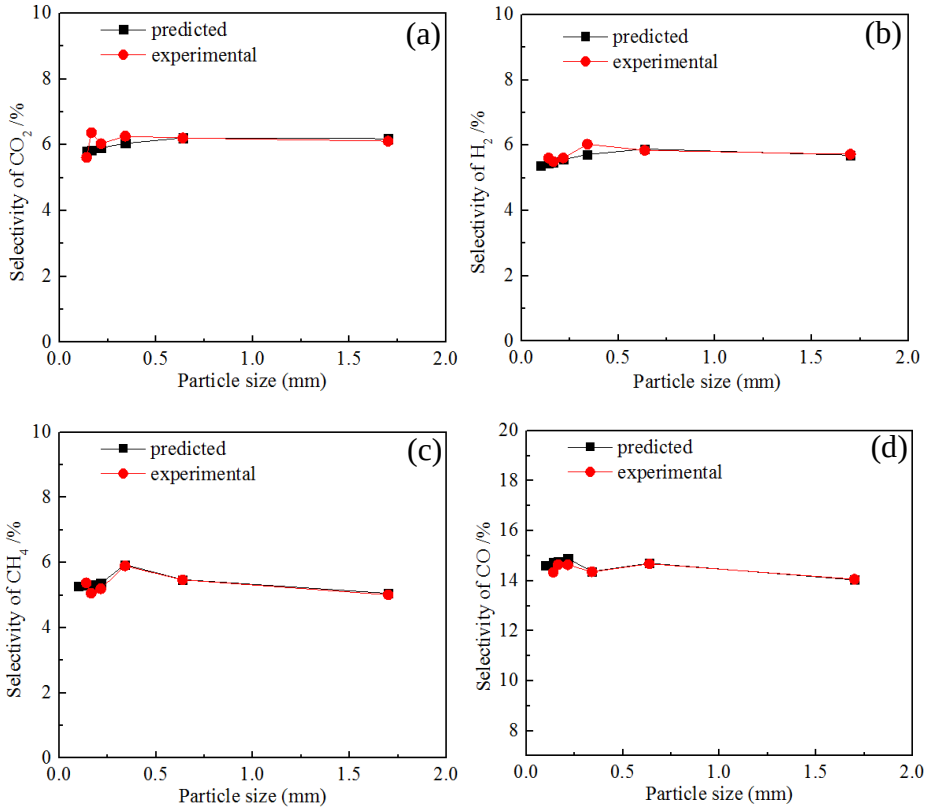

688

689

690 Fig. 10. Comparison between the experimental data (target output) and predicted
691 output data of the selectivity of CO_2 (a), H_2 (b), CH_4 and CO (d) with different
692 particle sizes in pyrolysis process. (Space velocity: 65 min^{-1}; Temperature: 800 ^oC)

693

694

695

696

697

698

699

700

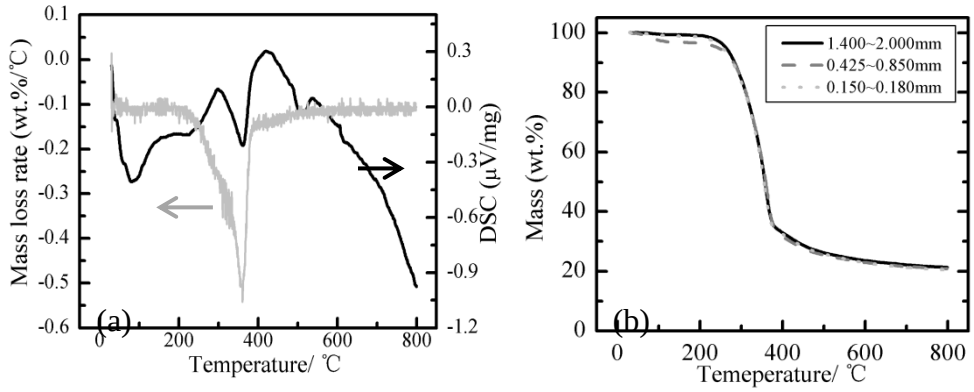

701

702 Fig. 11. DTG, DSC (a) and TG (b) curves of biomass for different particle sizes
703 (1.400~2.000 mm; 0.425~0.850 mm and 0.150~0.180 mm) at heating rate of
704 10℃/min.

705